Journal of Power Sources 246 (2014) 430–437

Contents lists available at ScienceDirect

Journal of Power Sources

journal homepage: www.elsevier.com/locate/jpowsour

Method for *in situ* carbon deposition measurement for solid oxide fuel cells

J. Kuhn, O. Kesler*

University of Toronto, Department of Mechanical and Industrial Engineering, 5 Kings College Rd., Toronto, ON, Canada M5S 3G8

HIGHLIGHTS

- A method for measuring carbon deposition in SOFC anodes *in situ* is developed.
- Only carbon deposits that have intimate contact with nickel can be gasified.
- >99.8 mass % of carbon with residence times up to 100 h can be gasified.
- Quantification of gasified carbon shows good agreement with TGA measurements.
- The observed effect of increased steam content is in agreement with the literature.

ARTICLE INFO

Article history:
Received 30 May 2013
Received in revised form
17 July 2013
Accepted 27 July 2013
Available online 7 August 2013

Keywords:
Solid oxide fuel cell
Carbon deposition
Coking
Nickel
Steam
Quantification

ABSTRACT

Previous methods to measure carbon deposition in solid oxide fuel cell (SOFC) anodes do not permit simultaneous electrochemical measurements. Electrochemical measurements supplemented with carbon deposition quantities create the opportunity to further understand how carbon affects SOFC performance and electrochemical impedance spectra (EIS). In this work, a method for measuring carbon *in situ*, named here as the quantification of gasified carbon (QGC), was developed. TGA experiments showed that carbon with a 100 h residence time in the SOFC was >99.8% gasified. Comparison of carbon mass measurements between the TGA and QGC show good agreement. *In situ* measurements of carbon deposition in SOFCs at varying molar steam/carbon ratios were performed to further validate the QGC method, and suppression of carbon deposition with increasing steam concentration was observed, in agreement with previous studies. The technique can be used to investigate *in situ* carbon deposition and gasification behavior simultaneously with electrochemical measurements for a variety of fuels and operating conditions, such as determining conditions under which incipient carbon deposition is reversible.

1. Introduction

Solid oxide fuel cells (SOFC) are high temperature (550–1000 °C) electrochemical devices that generate combined heat and electricity with potential system efficiencies nearly double that of combustion based energy systems. SOFCs can consume relatively low cost and readily available fuels such as methane. Methane can be directly fed to the fuel cell together with steam in a process called direct internal reforming (DIR), which improves system efficiency and reduces system cost compared to externally reforming the fuel prior to its use in the fuel cell [1]. DIR is made possible by the fact that part of the SOFC anode is commonly composed of Ni, a material frequently used for industrial steam reforming and cracking catalysts [2].

Traditional yttria-stabilized-zirconia (Ni–YSZ) anodes are susceptible to coking when exposed to dry hydrocarbon fuels at SOFC operating temperatures. The formation of solid carbon is the result of an imbalance between competing formation and gasification reactions [3]. Atomic carbon (C_α) deposits originate from the dissociation of hydrocarbons and CO, which creates various morphologies of carbon that block pores and reactive sites [4], cause metal dusting [5,6], bulk expansion [7], and fracturing of electronic and ionic conducting pathways [8]. Carbon deposition can be suppressed by feeding large amounts (>60 vol%) of steam with the fuel. However, large steam concentrations reduce the Nernst potential, efficiency, and SOFC performance. External steam generators and associated water storage increase system cost and complexity, and prevent SOFCs from being well-suited for

* Corresponding author. Tel.: +1 416 978 3835; fax: +1 416 978 7753.
E-mail addresses: joel.kuhn@mail.utoronto.ca (J. Kuhn), kesler@mie.utoronto.ca (O. Kesler).

0378-7753/$ – see front matter © 2013 Elsevier B.V. All rights reserved.
http://dx.doi.org/10.1016/j.jpowsour.2013.07.106

transportation and remote power applications. Therefore, it is useful to understand how Ni-based anodes perform under drier conditions.

A number of anode material sets have been developed to minimize or eliminate carbon deposition from directly feeding dry hydrocarbon fuels, including using precious metals such as Ru with Ni [9], scandia-stabilized-zirconia (ScSZ) instead of YSZ [10], infiltrated Cu and CeO_x [11], ceramic-based anodes [12], and nickel/gadolinia-doped-ceria (Ni–GDC) anodes [13]. However, many of these solutions use rare earth materials that have increased in price over recent years due to a reduction in Chinese export quotas [14]. BaO nanoislands on traditional Ni–YSZ anodes have been shown to promote water-mediated carbon removal reactions that create stable electrochemical performance in dry C_3H_8 for at least 100 h [15]. However, depositing a thin film of BaO on metal supported SOFCs is difficult due to the high temperatures required. Thus, in order to design a metal supported fuel cell with Ni-based anodes, an understanding of coking conditions is still important. Because operating conditions have a great influence on coking in SOFC anodes, a technique that can be used to quantify carbon deposition while operating the cells at various conditions is of great interest for aiding in the design of more robust anode compositions, microstructures, or operating regimes. The technique should be applicable to nickel-based anodes as well as to anodes that either contain decreased amounts of nickel or only alternative materials, and it can be used to determine the effectiveness and stability against coking of proposed new anode compositions or designs.

Tools commonly employed for carbon deposition studies include thermogravimetric analysis (TGA) [4,7,10,16], evolved gas analysis (EGA) [17–19], and Raman spectroscopy [20]. In TGA setups, it is difficult to provide two different gas streams and 4 electrodes to the anode and cathode while minimally disrupting the mass measurements, and Raman spectroscopy is limited to mapping regions in which carbon is prevalent, as opposed to quantification. However, EGA can be used to both quantify the total carbon and to characterize the morphology using temperature programmed oxidation (TPO) [8,21–24] or hydrogenation (TPH) [25].

Quantification of carbon *in situ* in SOFCs creates the opportunity to gain insight into the relationship between carbon deposits and resulting degradation of performance, electrochemical impedance changes, and anode morphological changes. TPO cannot be used for *in situ* quantification of carbon because nickel is oxidized in addition to the carbon, and oxidation of nickel causes another SOFC degradation mode known as redox cycling [26]. Additionally, thermal cycling that results from repeated TPO or TPH would also cause cell degradation. As a result, a new, less destructive method must be developed.

A specific form of EGA, defined here as the quantification of gasified carbon (QGC) method, involves feeding a carbon gasification agent at a fixed temperature and integrating the evolved carbon mass flow over the gasification period. Gasification occurs when a gasification agent is introduced via the reactions listed in Table 1.

Table 1
Carbon gasification reactions.

(1) $C(s) + O_2 \Rightarrow CO_2$
(2) $2C(s) + O_2 \Rightarrow 2CO$
(3) $C(s) + CO_2 \Rightarrow 2CO$
(4) $C(s) + 2H_2 \Rightarrow CH_4$
(5) $C(s) + H_2O \Rightarrow CO + H_2$
(6) $C(s) + 2H_2O \Rightarrow CO_2 + 2H_2$

First, different gasification agents were surveyed for their propensity to oxidize nickel and applicability to the QGC method using thermodynamic calculations and experiments. CO_2 and H_2 were then evaluated for their ability to completely gasify carbon with up to 100 h of residence time in the SOFC anode prior to gasification. Next, the accuracy of the QGC method was assessed using coupled TGAEGA. Finally, *in situ* carbon measurements on an SOFC at varying molar steam/carbon ratios (*S*/*C*) were determined and found to match well with trends reported in the literature, thus further verifying the QGC method.

2. Experimental procedure

Three sets of experiments were performed: chemical reversibility of deposited carbon after 100 h (TGA), validation of the QGC method (TGA–QGC), and *in situ* measurement of carbon deposition (QGC–SOFC test equipment). All thermogravimetric analyses were performed using a Setaram Setsys 1750 CS Evolution TGA. An external manual 3-way valve was installed on the auxiliary gas port so that H_2 could be used with either CH_4, C_2H_6, or CO. *Ex situ* masses were measured using a Mettler Toledo AB204-S/FACT digital balance. The concentration of CO was measured using a Thermo Scientific Model 48i Gas Filter Correlation CO Analyzer containing an internal volumetric flow meter. Flow rates and CO measurements from the CO analyzer were calibrated using a gas delivery system produced in-house and a 1% CO/balance N_2 gas bottle. The gas delivery system is part of a complete SOFC test apparatus also produced in-house. H_2 was generated using a Parker Balston H2-800NA electrolyzer, and all bottled gases were acquired from Linde Canada.

2.1. Choice of QGC gasification agent

The choice of a gasification agent for the QGC method was based on thermodynamic equilibrium calculations and on the practicality of measuring evolved carbonaceous species. Equilibrium calculations helped determine both the gasification temperature and the propensity for NiO formation from exposure to the gasification agent. Chemical equilibrium constants for carbon gasification reactions (Table 1) and NiO producing reactions (Table 2) were calculated using Matlab R2008b as a front-end for the publicly available NASA-CEA equilibrium solver [27]. C(gr) represents graphite, and C(s) represents all solid phase carbon.

In addition to the thermodynamic equilibrium calculations, the oxidation kinetics of carbon and nickel were evaluated to test the viability of O_2 as a QGC gasification agent. 90 mg of graphite powder and 39.8 mg of nickel powder were used in the TGA. Nickel powder was produced by pre-reducing NiO powder (Novamet) with a D50 size by volume of 16 μm in a tube furnace. The graphite powder used (Alfa Aesar) falls in a sieve fraction of 171–841 μm. The temperature in the TGA was ramped to 900 °C at 1 °C min^{-1} with an air flow rate of 200 sccm.

Table 2
Reactions that generate NiO.

(1) $Ni + CO_2 \Rightarrow NiO + CO$
(2) $2Ni + CO_2 \Rightarrow 2NiO + C(s)$
(3) $Ni + CO \Rightarrow NiO + C(s)$
(4) $2Ni + O_2 \Rightarrow 2NiO$
(5) $Ni + H_2O \Rightarrow NiO + H_2$

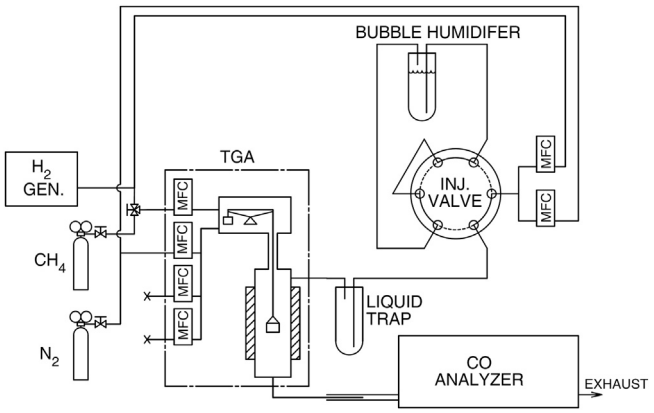

Fig. 1. Schematic of configuration used to validate QGC method.

2.2. Chemical reversibility of deposited carbon after 100 h

In order for the QGC method to correlate deposited carbon with changes in cell performance, all deposited carbon must be removable for complete characterization, even after significant residence times (e.g. 100 h). Chemical reversibility tests (named in the fuel cell context where electrochemical reversibility is also possible) were performed in the TGA using slices of 1/6 button half-cells (anode-electrolyte structures) directly suspended from a gold wire. The button half-cells, produced elsewhere [28], consisted of a Ni/YSZ support, Ni/ScSZ anode functional layer, and ScSZ electrolyte (total thickness 1 mm). The sample mass was measured *ex situ* before and after testing in the TGA. The schematic of the setup is shown in Fig. 1 (water injection assembly and CO analyzer were not used for the chemical reversibility experiment). Each sample was suspended and heated to the intended operating temperature (600 or 700 °C) at 5 °C min^{-1} in 4% H_2/balance N_2. The H_2 feed rate controlled by the auxiliary gas mass flow controller (MFC) was then reduced to 0.75 sccm while the N_2 flow rate was fixed at 200 sccm. When the balance stabilized, the auxiliary gas was switched from H_2 to the carbon deposition gas (CH_4, C_2H_6, or CO). The low concentration of fuel gas (~0.4%) resulted in an accumulation of carbon over 100 h. When the deposition phase was complete, the gasification agent (CO_2 or H_2) was introduced. The experimental conditions and results are summarized in Table 3.

2.3. Validation of the QGC method

Validation of the QGC method was performed in the TGA using anode supported button cell chips in a 170 μl alumina crucible suspended from a gold wire with a CO analyzer coupled to the exhaust. Anode supported button half-cells were purchased from the Ningbo Institute of Materials Technology and Engineering (NIMTE) and chipped with pliers to form pieces that fit inside the crucible. The cells consist of a ~385 μm thick nickel and YSZ support, ~10 μm nickel and YSZ functional anode layer, and ~20 μm YSZ electrolyte. The schematic of the setup used for QGC validation studies is depicted in Fig. 1. The chipped NIMTE half-cell was ramped to 700 °C in 4% H_2/balance N_2 and reduced overnight (12 h). Carbon was deposited on the reduced cell by switching the auxiliary gas from H_2 to CH_4 until 5–20 mg of carbon was deposited. Then the auxiliary gas was switched back to H_2 for ~30 min, and dry N_2:H_2 (290:10 sccm) was turned on to help purge the TGA furnace of CH_4 while preserving the carbon [29]. When the TGA mass signal stabilized, the injector valve was actuated to bubble humidify the N_2:H_2 mixture. The experiment was terminated when the mass signal stabilized after gasification was complete. Excess liquid from bubble humidification was separated using a liquid trap. The pumping rate of the CO analyzer is fixed (~1000 ml min^{-1}), and therefore, external air is drawn in with the CO-rich sample stream exiting the TGA, since the flow rate of the sample stream was lower than the fixed flow rate of the analyzer. The flow rate and concentration values read by the CO analyzer were calibrated directly before performing the validation run.

2.4. In situ measurement of carbon deposition

For further validation of the QGC method, *in situ* carbon deposition measurements were performed on full NIMTE button cells using a gas delivery system and button cell sample holder produced in-house. The sample holder was heated in a Carbolite-VST vertical split tube furnace. High humidity was generated with a Bronkhorst liquid mass flow controller and custom-built evaporator. The cells were sealed to the sample holder using Flexitallic Thermiculite® 866 vermiculite gaskets. The temperature of the cell was determined by a thermocouple that resides ~4 mm axially from the cathode surface. During the CH_4 exposure, the furnace temperature was increased to compensate for cooling due to steam reforming in order to keep the cell thermocouple reading constant. A flow rate of 20 sccm N_2 was used at the cathode during carbon deposition to prevent unintended carbon gasification by air crossover or electrochemical removal of carbon by O^{2-} ions. After CH_4 and H_2O exposure for 10 h, the cell was purged of CH_4 and H_2O using N_2 and H_2 at 195 & 5 sccm, respectively, for 30 min. Then, carbon was gasified with bubble humidified N_2 and H_2 at 290 & 10 sccm, respectively.

3. Results and discussion

3.1. Choice of gasification agent

O_2, CO_2, H_2, and H_2O are all known to have the ability to gasify solid carbon on nickel [4,16,30,31]. H_2O and CO_2 are commonly studied in the gasification of coal and char [32–34]. An important

Table 3
Summary of deposition and gasification conditions in the TGA for chemical reversibility testing.

Test ID	Temp. [°C]	Deposition gas composition	Deposition gas flow rate [sccm]	Gasification gas composition	Gas flow rate [sccm]	Start mass [mg]	End mass [mg]	Mass change [mg]	Mass change [%]
1	700	N_2:CH_4	200:1	CO_2:H_2	148:8	397	396.6	−0.4	−0.101
2	600	N_2:CH_4	200:0.75	CO_2:H_2	148:8	365.4	365.4	0.0	0.000
3	700	N_2:CH_4	200:0.75	N_2:H_2	200:8	244.5	244.3	−0.2	−0.082
4	600	N_2:CH_4	200:0.75	N_2:H_2	200:8	366.9	367.6	0.7	0.191
5	600	N_2:CO	200:0.75	CO_2:H_2	148:8	358.3	357.6	−0.7	−0.195
6	700	N_2:CO	200:0.75	CO_2:H_2	148:8	351.9	351.4	−0.5	−0.142
7	700	N_2:C_2H_6	[a]200:0.75	CO_2:H_2	148:8	372	372	0.0	0.000
8	600	N_2:C_2H_6	200:0.75	CO_2:H_2	148:8	348	347.8	−0.2	−0.057

[a] Reduced C_2H_6 flow rate to 0.3 sccm @ 71.68 h of deposition step.

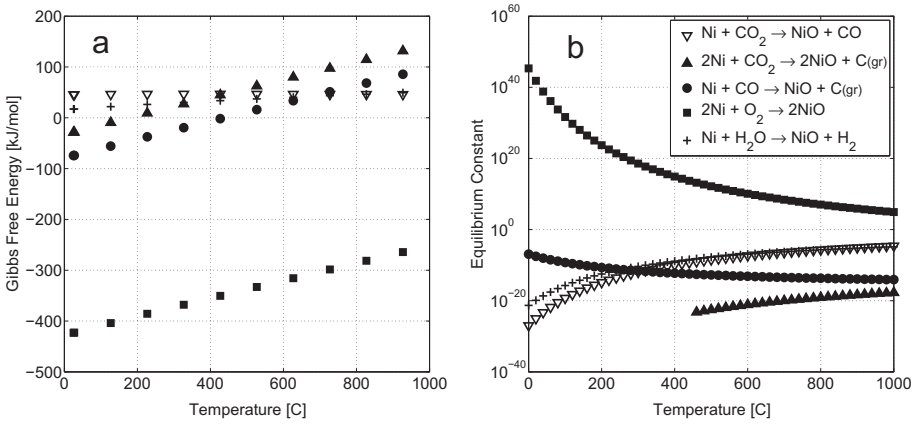

Fig. 2. a) Gibb's free energy and b) equilibrium constants for NiO producing reactions listed in Table 2.

characteristic of the gasification agent is that it must not re-oxidize nickel. Re-oxidation of nickel changes the morphology of the nickel cermet and potentially degrades cell performance [26,35,36]. Nickel in SOFC anodes has been observed to re-oxidize under high fuel utilization conditions where the gas mixture contains high levels of CO_2 and H_2O [37].

The results of Gibb's free energy and thermodynamic equilibrium calculations for NiO producing reactions are shown in Fig. 2. Note that the equilibrium solver was not able to converge at temperatures lower than 460 °C for reaction 2. In general, the reactions listed in Table 2 are endothermic in the range of 0–1000 °C with the exception of reaction 3 below ~400 °C and reaction 4. Based on the thermodynamic equilibrium calculations, CO_2, CO, and H_2O will not create a significant amount of NiO at SOFC operating temperatures. However, for reaction 4, NiO formation is thermodynamically favored with an increasing propensity at lower temperatures, similarly to oxidation of graphite with O_2 [30].

O_2 was eliminated as a gasification agent because the kinetics of nickel oxidation is faster than that of graphite oxidation (Fig. 3). Robinson et al. [38] observed oxidation of Ni nanocrystallites at approximately 320 °C, similarly to the observation of the TGA experiment here. Although oxidation rates are largely controlled by particle sizes [39], this TGA experiment confirmed previous results that nickel in an SOFC would be susceptible to rapid oxidation if O_2 were used as a gasification agent for the cell microstructure used.

The equilibrium constants for the carbon gasification reactions 3–6 are shown in Fig. 4. Reactions 3–5 favor the products at high temperatures, while the methanation reaction favors products at low temperatures. The plots intersect unity at approximately 533, 617, 660, and 670 °C for the steam gasification (product CO_2), steam gasification (product CO), methanation, and reverse Boudouard reactions, respectively. The reverse Boudouard and steam gasification reactions are better suited for gasification at $T \geq 700$ °C, where they have faster kinetics and are increasingly product favored, in contrast to the methanation reaction, which is less favored at $T \geq 700$ °C.

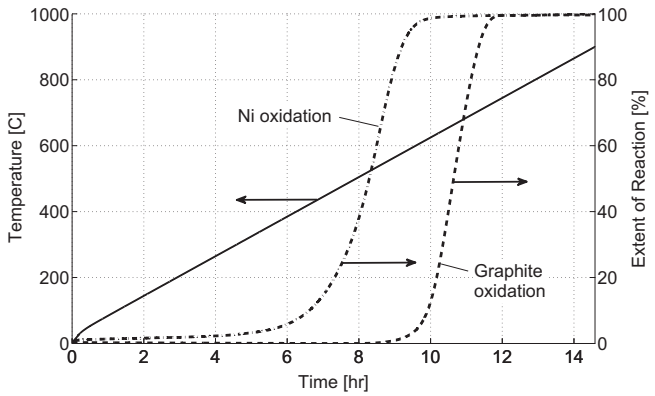

Fig. 3. Comparison of Ni and graphite oxidation using the TGA.

Although theoretically, CO_2, H_2, and H_2O can all be used for safe gasification of carbon, the choice of an ideal gasification agent for the QGC method depends on the method used to measure the products. H_2 has the advantage of acting as a fuel and oxidation preventative while gasifying carbon on an operating SOFC, but ppmv level detection of methane is difficult in a mass spectrometer, because fractions of water (that are continuously recycled within the vacuum chamber) pollute the signal at $m/z = 16$, where methane is measured. CO_2 gasification is fast at 700 °C, CO_2 is easy to feed, and low levels of CO can be easily measured using a nondispersive infrared (NDIR) CO analyzer, but low percent levels of H_2 (fed with CO_2 to prevent the O_2 impurities from oxidizing the nickel) cause the reverse water–gas shift reaction to generate CO and skew the measurement. Using steam as a gasification agent circumvents the problem of the water–gas shift reaction, but can result in both CO and CO_2 as products (indicated in Fig. 4), and it can be difficult to feed because of its low temperature condensation point. Nonetheless, if the ratio of CO:CO_2 in the product stream is high due to gasification kinetics, H_2O is the best choice for gasification agent because CO is easily detected and quantified using an NDIR CO analyzer. Furthermore, unlike H_2 gasification, the reaction rate can be increased by raising the gasification temperature. Gasification rates for each of the reactants H_2, CO_2, and H_2O were further analyzed by 100 h chemical reversibility testing.

3.2. Chemical reversibility of deposited carbon after 100 h

Carbon diffusion into bulk nickel metal is intrinsic to the mechanism that forms vermicular carbon, C_v, and causes metal dusting [3,5,40,41]. When carbon is trapped beneath the surface of the metal, the area of carbon exposed to the pore, where potential gasification agents can remove it, is decreased. Furthermore, when carbon diffuses into nickel, the nickel metal helps to catalyze the formation of a morphology of carbon that has a higher crystallinity and stability than carbon deposits formed on the surface. Carbon in this state is more difficult to remove than other forms, such as C_α or C_v. Theoretically, both reduced access to gasification agents and high carbon crystallinity should decrease the reversibility of the carbon deposit. The time dependent nature of diffusion also

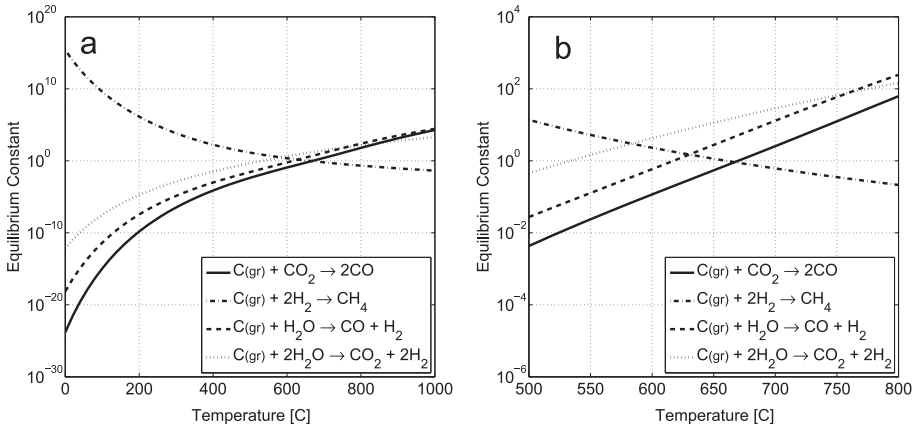

Fig. 4. Equilibrium constants for carbon gasification reactions from a) 0–1000 °C and b) 500–800 °C. Equilibrium constant for gasification using O_2 was too large to properly converge.

suggests that there would be a higher amount of irreversible carbon (unremovable) after longer exposures to carbonaceous fuel mixtures.

A complete summary of the change in mass over time during carbon deposition and gasification is shown in Fig. 5. The gap seen in Fig. 5a during carbon deposition is due to an unexpected restart of the TGA control computer. However, the TGA conditions were unaltered by the shutdown and a new datafile was restarted to finish the test. The plot was stitched together by knowing the shutdown time and linear extrapolation from the deposition rate before the shutdown. Also, in Fig. 5c, the carbon deposition rate was

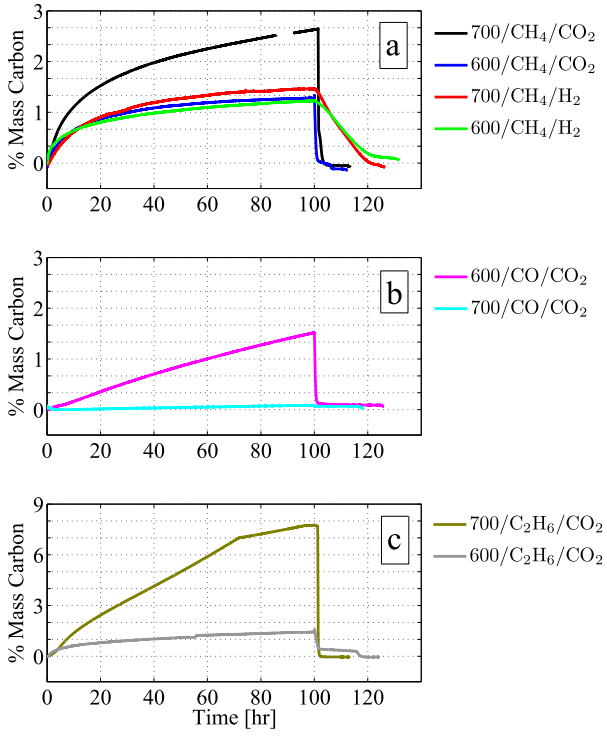

Fig. 5. Summary of carbon deposition and gasification results for 100 h chemical reversibility testing for carbon deposition from (a) CH_4, (b) CO, and (c) C_2H_6. Conditions for each test are summarized in Table 3. Each plot is labeled by the operating temperature in °C, carbon deposition gas, and gasification agent, respectively. Carbon mass is normalized by the total mass of the reduced sample. Note the different scale for plot (c).

so high that the C_2H_6 flow rate was reduced to prevent the suspended sample from falling due to bulk expansion of the porous nickel. Nonetheless, the electrolyte of the cell in Fig. 5c was severely cracked and irreversibly damaged. The mass changes in Fig. 5 are normalized by the mass of the reduced samples before exposure to carbon. Ideally, the surface area of the nickel should be used for normalization; however, pulsed CO chemisorption experiments (not shown) were not sensitive enough to measure the low surface areas of the nickel in the samples.

In general, all half-cell slices experienced a trend of decreasing rate of carbon formation over the 100 h period. This observation is in agreement with the one by Refs. [4,42], who explained the trend as a result of increasing encapsulation of nickel by carbon. Another observation is that the methane experiments 2–4 in Fig. 5a had identical deposition atmospheres but different temperatures and ended up with similar levels of carbon after 100 h. Furthermore, experiment 1, which used a slightly higher methane feed rate of 1 sccm, deposited a higher level of carbon than experiments 2–4. At low CH_4 partial pressures, it is apparent that carbon deposition rates are more sensitive to the CH_4 partial pressure than to temperature. The trends in carbon deposition from C_2H_6 are similar to those from CH_4; however, at 700 °C, there are nearly linear carbon formation rates in the last 50 h of carbon deposition. Carbon deposition rates from C_2H_6 are also more sensitive to temperature than those from CH_4. It has been proposed that carbon deposition on Ni/YSZ cermets from C_2H_6 occurs as a result of both heterogeneous and homogeneous decomposition [43].

Carbon deposition rates from CO were linear over a longer range of time than carbon deposition from hydrocarbons, as seen in Fig. 5b. Carbon deposition from CO requires fewer active nickel sites per molecule of CO than carbon deposition from hydrocarbons, and therefore is less sensitive to encapsulation [44]. The total amount of carbon from CO at 700 °C was the lowest of all experiments, which is primarily a result of the Boudouard reaction being reactant favored at 700 °C (Fig. 4).

Referring to Table 3, in general, greater than 99.8% of deposited carbon could be removed by H_2 and CO_2 at 700 °C. Experiments 1, 3, 5, 6, and 8 all saw negative weight changes that might suggest that nickel particles separated from the bulk by metal dusting and dropped from the suspended sample. This hypothesis was further explored in another test in which the reduced sample was broken up to fit completely within an alumina crucible. However, a negative weight change was still observed. It could also be explained by anodes that were incompletely reduced or by the precision of the *ex situ* balance. The exact cause remains unclear.

Chen et al. [45] and Novosel et al. [46] both observed vermicular carbon, encapsulating carbon, carbon diffused into bulk nickel, and a shift towards less surface carbon at higher temperatures. Greater than 99.8% of carbon gasified after 100 h suggests that carbon is not trapped in the bulk of the nickel. Either carbon can rapidly diffuse to the surface or most of the carbon deposit resides near the surface. It is also possible that a relatively small amount of carbon is trapped in the bulk, with its weight masked by the mechanism that causes the negative weight change.

Several results were observed from the gasification phase of the experiments. In general, gasification rates rose very rapidly (achieving maximum gasification rate in less than 1 min) and decayed slowly as the carbon was removed. For CO_2 at 700 °C, complete gasification occurred in ~2–4 h, and the peak gasification rates ranged from ~0.2–2 mg min^{-1}. Whereas with CO_2 at 600 °C, complete gasification did not occur within 2–4 h unless the temperature was increased to 700 °C, where the reverse Boudouard reaction is more favored. Interestingly, a second peak in the gasification rate (with lower magnitude than the primary peak) occurred ~1–2 h after the primary peak for samples 1 & 8. This result may be due to the opening of pore space that allows better access to trapped carbon. It could also be the result of surface carbon (vermicular or otherwise) being gasified first, while carbon that diffused into the bulk nickel must diffuse back to the surface before gasification.

Gasification with 4% H_2 yielded very low gasification rates ($<4 \times 10^{-3}$ mg min^{-1}). In experiments 3 and 4, complete gasification required more than 20 h. However, the work of Trimm and Bernardo [16] showed the methanation reaction rate to be equal to or greater than CO_2 gasification rates between 650 and 700 °C. To see how the concentration of H_2 affects the methanation rate, two tests (at 600 & 700 °C) were conducted in the TGA using 100% H_2 as a gasification agent. After verifying that the TGA was leak tight, 15.56 and 17.45 mg (4.6 & 5.2% weight gain) of carbon were deposited at 700 and 600 °C, respectively. Both carbon deposits were completely gasified and the gasification rates peaked at 1.07 and 0.92 mg min^{-1} at 700 and 600 °C, respectively. This result demonstrates that the low gasification rates observed with 4% H_2 were due primarily to the low concentration of H_2. Additionally, experiments 3 and 4 also show that N_2 with low concentrations of H_2 (<1 vol%) works well to preserve carbon deposited in the cell.

3.2.1. Carbon deposition from the homogeneous Boudouard reaction

In Fig. 5b it can also be seen that both experiments appear to leave carbon ungasified despite the *ex situ* masses having negative mass changes. In these two cases, the Boudouard reaction proceeded homogeneously and deposited carbon on the gold suspension wire that was not removed by CO_2 gasification. To further explore this result, two tests were performed using the same gold suspension wire with an empty alumina crucible hanging from it. The temperature was ramped to 800 °C at 3 °C min^{-1} while flowing gas mixtures containing CO. The conditions and results are seen in Table 4.

In both experiments, the mass began to increase at approximately 400 °C. Even more interesting is that the addition of H_2 increased the total amount of carbon deposited by approximately a factor of three. Such an increase has been experimentally observed on nickel based anode materials [21]. Density functional theory (DFT) calculations have shown that a COH intermediate reduces the activation energy required at nickel step sites [47,48]. However, it is unclear how hydrogen may accelerate the homogeneous Boudouard reaction. Nonetheless, carbon precipitating from homogeneous reactions on the SOFC test fixture surfaces surrounding the cell causes QGC measurements to read higher amounts of carbon than were deposited on the cells due to gasification of some of the non-cell carbon. Gasification of non-cell carbon may only be partially complete due to lack of a catalyst. Decomposition of higher hydrocarbons (ethane, propane) may present similar problems.

Table 4
Homogeneous Boudouard reaction TGA experiments.

Test ID [−]	Gas composition [−]	Flow rates [sccm]	Weight gain [mg]	Conversion [%]
1	N_2:CO	200:15	0.05	4.78
2	N_2:CO:H_2	195:15:5	0.169	16.17

3.3. Validation of the QGC method

The accuracy of the QGC method must be evaluated before performing *in situ* measurements. Calculated QGC measurement uncertainties are only controlled by the measurement uncertainties of a volumetric flow meter [49]. There are a number of things that can affect the accuracy of the QGC validation experiment. First, if the TGA is not properly flushed of residual CH_4 from the deposition step, steam reforming can occur and generate higher than expected CO levels. Second, calibration of the CO analyzer is critical because it can cause an underestimation or overestimation of gasified carbon. For example, the calibration is affected by the purity of the calibration gas. Calibrations with a CO bottle near expiration caused carbon measurements that were higher than expected based on the TGA measurements. Calibration using a fresh 1% CO/balance N_2 mixture cylinder gave improved results. The mass flow rate of carbon (mg min^{-1}) passing through the CO analyzer is calculated using Equation (1).

$$\dot{m}_C = \dot{V}\rho_{CO}\left(\frac{C_{CO}}{1E6}\right)\left(\frac{MM_C}{MM_{CO}}\right) \quad (1)$$

Here, $\dot{V}$ is the volumetric flow rate at standard conditions (0 °C, 101.3 kPa) through the analyzer in sccm (calibrated), ρ_{CO} (1.249 mg ml^{-1}) is the density of carbon monoxide at standard conditions, C_{CO} is the concentration of CO in ppmv (calibrated), and MM_C and MM_{CO} are the molar masses of carbon and carbon monoxide, respectively. With Equation (1), the CO concentration and flow rates recorded as a function of time were directly

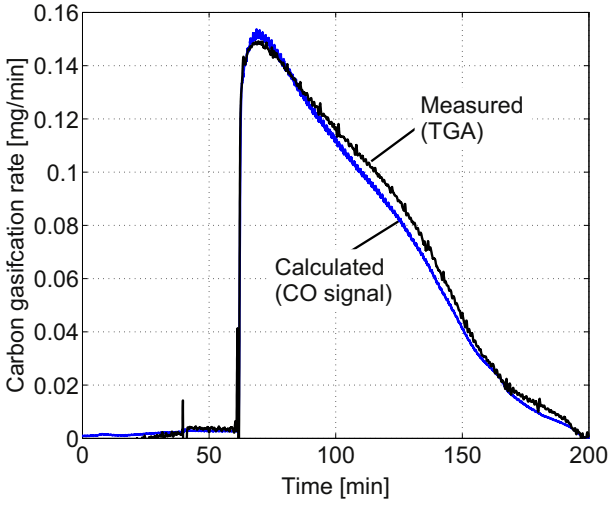

Fig. 6. QGC validation: comparison of the first derivative of the TGA mass signal and the calculated carbon removal rate from the evolution of CO as measured by the CO analyzer.

converted into a mass flow rate versus time that could be numerically integrated to find the total amount of gasified carbon.

Very good agreement between the first derivative of the TGA mass signal and the calculated carbon gasification rate from the evolved CO was obtained, as can be seen in Fig. 6. The first derivative of the mass signal was generated in the TGA software (Calisto Processing v1.077) using a derivative filter of 60 s. The CO concentration and flow rate signals from the CO analyzer were used to compute the gasification rate of CO using Equation (1). For the purpose of comparison, the signals were aligned by their respective rapid inclines at the beginning of the gasification step.

The change in mass calculated in the TGA was 10.328 ± 0.00002 mg, and numerical integration of Equation (1) resulted in a value of 9.89 ± 0.20 mg. The value calculated by the QGC method was approximately 4.3% lower than the TGA value. Theoretically, the remaining carbon may have evolved as CO_2, particularly in the time between 100 and 150 min where the CO signal is lower than the TGA derivative. Because any CO_2 evolving from the cell was found from the results in Fig. 6 present at a concentration of less than 5%, it is proposed that the kinetics of CO_2 production from CO (heterogeneous or homogeneous) are slow, despite thermodynamic equilibrium calculations suggesting that CO_2 is the dominant product over CO. The H_2 content of the bubble humidified gasification agent (N_2:H_2:H_2O) might also convert produced CO_2 back to CO via the reverse water–gas shift reaction. Finally, it was observed that H_2O was capable of complete gasification of carbon deposited on nickel, similarly to the observations from the 100 h chemical reversibility experiments. In kinetic studies of the carbon deposition and gasification rates, coincident measurement of evolved CO_2 with CO would be required. However, when using the QGC method for detecting the existence of carbon *in situ* to find a boundary between carbon and no-carbon precipitating gas mixtures, the method was shown to be valid.

3.4. In situ measurement of carbon deposition

To illustrate the use of the technique, *in situ* carbon deposition experiments were performed on the NIMTE fuel cells. Fig. 7 shows the results of *in situ* carbon deposition measurements at 700 °C for varying *S*/*C* ratios. The measured OCV before carbon deposition ranged between 1.112 and 1.116 V, ~3–7 mV below the theoretical Nernst potential. Good agreement between the measured OCV and theoretical Nernst potential, such as the values reported here, implies both accurate temperature control and minimal mixing between the fuel and oxidant compartments. Carbon was detected both below and above the carbon deposition boundary $S/C = 1.183$ predicted by thermodynamic equilibrium calculations. However, below $S/C \sim 1.28$, it was observed that increases in *S*/*C* caused decreases in carbon deposition. Above $S/C \sim 1.28$, carbon deposition is suppressed to very low values, and the *S*/*C* has less of an effect on carbon deposition compared to below $S/C \sim 1.28$. Furthermore, carbon deposition cannot be fully eliminated within the range of *S*/*C* ratios used. It is conjectured that carbon measured at $S/C > 1.28$ is the result of CO and CH_4 concentration gradients created by the porosity in the cermet leading to locally favorable deposition conditions. It is also conjectured that surface carbon is trapped at an intermediate stage of steam reforming due to the removal of steam during the purge step. Further exploration of carbon deposition boundaries will be performed in future work.

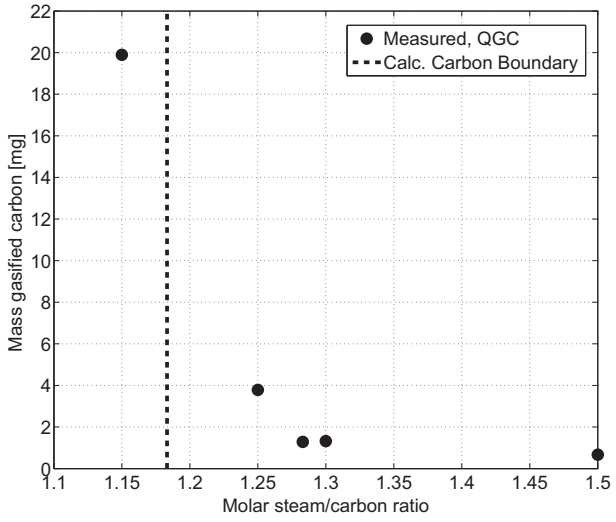

Fig. 7. *In situ* carbon deposition measurements at different *S*/*C* ratios using the QGC method at 700 °C. The dashed line represents the calculated threshold to carbon deposition based on thermodynamic equilibrium.

The technique can be applied to both nickel-based anodes or anodes with other compositions in studies of the effect of modified microstructures or operating conditions on coking. It can also be applied to anodes with compositions that are modified to increase their stability against coking in hydrocarbon fuels. Such anodes, for example, may include both anodes with lower amounts of nickel than in standard anodes, such as copper or ceramic-based anodes with nickel added in small amounts as a catalyst but not as the percolated electronic conducting phase, or entirely ceramic or copper-based anodes without any nickel added. Such studies will be included in future applications of the technique introduced in this work.

3.5. QGC method limitations

It is important to note that the accuracy of the QGC method is dependent on the intimacy of the contact between the catalyst and deposited carbon. In a separate set of experiments, CO_2 and H_2 gasification were explored with graphite powder, a dry mixture of nickel and graphite powder, and nickel-coated graphite in the TGA. The nickel and graphite were the same materials as described in Section 2.1. Ni coated graphite powder was prepared by using a $Ni(NO_3)_2 \cdot 6H_2O$ (Alfa Aesar) solution that created ~26 wt% (by total mass) Ni metal loading after decomposition. Although some gasification occurred with all samples, none of them experienced a complete gasification of carbon. The Ni-coated graphite powder sample showed the highest amount of gasified carbon, but the gasification mechanism was deactivated before all carbon could be gasified. Thus, the QGC method is limited to gasification of C_α, C_v, or carbon dissolved in the catalyst phase. Carbon that results from the homogeneous Boudouard reaction or decomposition of higher hydrocarbons (e.g. C_2H_6 [43]) that forms on non-catalyst sites has a prohibitively slow gasification rate.

4. Conclusions

Carbon deposition is a critical degradation mode for SOFCs that leads to changes in the morphology of the anode and irreversible damage. Measuring carbon *in situ* is integral to gaining a better understanding of how changes to material sets and operating conditions can prevent carbon deposition. The QGC method has been developed in this work to measure carbon deposition *in situ*. CO_2, H_2, and H_2O all have the capability to gasify carbon on nickel without the formation of NiO; however, gasification with H_2O is the most practical for the QGC method because the resulting CO can be accurately measured with an NDIR CO analyzer. It was observed that carbon is completely gasified only when it is deposited on a Ni cermet from CO or hydrocarbon decomposition. It was also

observed that >99.8% of carbon can reside on the Ni in the anode for up to 100 h and still be gasified. CO is the dominant product during H_2O gasification of carbon. It was found that the QGC method resulted in a carbon deposition measurement that was 4.3% lower than the gravimetric measurements, which is sufficiently accurate for resolving carbon deposition boundaries in SOFCs. The QGC method was applied to measure carbon *in situ*, and significant suppression of carbon deposition by steam was observed at $S/C > 1.28$.

A number of future research opportunities result from development of the QGC method. Correlations between deposited carbon content and performance degradation, electrochemical impedance changes, and anode morphological changes can be observed. The QGC method can also be used to study the amount of carbon required for electrolyte fracture. These examples and others will be explored in future work.

Acknowledgments

The authors gratefully acknowledge financial support from the Natural Sciences and Engineering Research Council (NSERC) of Canada, as well as from the Solid Oxide Fuel Cells Canada Strategic Research Network sponsored by NSERC and other sponsors listed at www.sofccanada.com. Donations of the gasket material by Flexitallic L.P. (Deer Park, TX, USA) are also greatly appreciated.

References

[1] R. Braun, S. Klein, D. Reindl, Journal of Power Sources 158 (2006) 1290–1305.
[2] C. Bartholomew, Encyclopedia of Catalysis, Wiley, 2006.
[3] D. Trimm, Catalysis Today 49 (1999) 3–10.
[4] J. Snoeck, G. Froment, M. Fowles, Industrial and Engineering Chemistry Research 41 (2002) 4252–4265.
[5] Z. Zeng, K. Natesan, Chemistry of Materials 15 (2002) 872–878.
[6] C. Chun, T. Ramanarayanan, Journal of the Electrochemical Society 154 (2007) C465–C471.
[7] Y. Kim, J. Kim, J. Bae, C. Yoon, S. Nam, Journal of Physical Chemistry C 116 (2012) 13281–13288.
[8] H. He, J. Hill, Applied Catalysis A 317 (2007) 284–292.
[9] T. Takeguchi, R. Kikuchi, T. Yano, K. Eguchi, K. Murata, Catalysis Today 84 (2003) 217–222.
[10] T. Iida, M. Kawano, T. Matsui, R. Kikuchi, K. Eguchi, Journal of the Electrochemical Society 154 (2007) B234–B241.
[11] S. Park, R. Craciun, J. Vohs, R. Gorte, Journal of the Electrochemical Society 146 (1999) 3603–3605.
[12] J. Liu, B. Madsen, Z. Ji, S. Barnett, Electrochemical and Solid-State Letters 5 (2002) 2002.
[13] K. Lee, C. Gore, E. Wachsman, Journal of Materials Chemistry 22 (2012) 22405–22408.
[14] S. Massari, M. Ruberti, Resources Policy 38 (2013) 36–43.
[15] L. Yang, Y. Choi, W. Qin, H. Chen, K. Blinn, M. Liu, P. Liu, J. Bai, T. Tyson, M. Liu, Nature Communications 2 (2011) 1–9.
[16] C. Bernardo, D. Trimm, Carbon 17 (1978) 115–120.
[17] H.S. Bengaard, J.K. Nørskov, J. Sehested, B.S. Clausen, L.P. Nielsen, A.M. Molenbroek, J.R. Rostrup-Nielsen, Journal of Catalysis 209 (2002).
[18] T. Osaki, T. Mori, Reaction Kinetics and Catalysis Letters 89 (2006) 333–339.
[19] B. Novosel, M. Avsec, J. Maček, Materiali in Tehnologije 42 (2008).
[20] M. Liu, K. Blinn, H. Abernathy, X. Li, M. Liu, L. Bottomley, Energy and Environmental Science 5 (2012) 7913–7917.
[21] V. Alzate-Restrepo, J. Hill, Journal of Power Sources 195 (2010) 1344–1351.
[22] K. Ke, A. Gunji, H. Mori, S. Tsuchida, H. Takahashi, K. Ukai, Y. Mizutani, H. Sumi, M. Yokoyama, K. Waki, Solid State Ionics 177 (2006) 541–547.
[23] A. Gunji, C. Wen, J. Otomo, T. Kobayashi, K. Ukai, Y. Mizutani, H. Takahashi, Journal of Power Sources 131 (2004) 285–288.
[24] J. Maček, B. Novosel, M. Marinšek, Journal of the European Ceramic Society 27 (2007) 487–491.
[25] K. Nikooyeh, R. Clemmer, V. Alzate-Restrepo, J. Hill, Applied Catalysis A General 347 (2008) 106–111.
[26] T. Klemenso, C. Chung, P. Larsen, M. Mogensen, Journal of the Electrochemical Society 152 (2005) A2186–A2192.
[27] B.J. McBride, S. Gordon, Computer Program for Calculation of Complex Chemical Equilibrium Compositions and Applications II [Online], 1996, http://www.grc.nasa.gov/WWW/CEAWeb/.
[28] X. Zhang, M. Robertson, S. Yick, C. Deĉes-Petit, E. Styles, W. Qu, Y. Xie, R. Hui, J. Roller, O. Kesler, R. Maric, D. Ghosh, Journal of Power Sources 160 (2006) 1211–1216.
[29] C. Li, Y. Shi, N. Cai, Journal of Power Sources 225 (2012) 1–8.
[30] A. Tomita, Catalysis Surveys from Japan 5 (2001) 17–24.
[31] D. Duprez, K. Fadili, J. Barbier, Industrial and Engineering Chemistry Research 36 (1997) 3180–3187.
[32] D. Roberts, D. Harris, Fuel 86 (2007) 2672–2678.
[33] L. Zhang, J. Huang, Y. Fang, Y. Wang, Energy and Fuels 20 (2006) 1201–1210.
[34] M. Irfan, M. Usman, K. Kusakabe, Energy 36 (2011) 12–40.
[35] T. Klemenso, C. Appel, M. Mogensen, Electrochemical and Solid-State Letters 9 (2006) A403–A407.
[36] D. Waldbillig, A. Wood, D. Ivey, Solid State Ionics, Diffusion & Reactions 176 (2005) 847–859.
[37] P. Nehter, Journal of Power Sources 164 (2007) 252–259.
[38] P. Robinson, V. Arun, S. Manju, C. Aniz, K. Yusuff, Journal of Thermal Analysis and Calorimetry 100 (2010) 2.
[39] R. Karmhag, G. Niklasson, M. Nygren, Journal of Applied Physics 85 (1999) 2.
[40] J. Figueiredo, C. Bernardo, J. Chludzinski Jr., R. Baker, Journal of Catalysis 110 (1988) 127–138.
[41] C.H. Bartholomew, Catalysis Reviews 24 (1982) 67–112.
[42] J. Snoeck, G. Froment, M. Fowles, Journal of Catalysis 169 (1997) 240–249.
[43] G. Glasier, P. Pacey, Carbon 39 (2001) 15–23.
[44] A.K. Avetisov, J.R. Rostrup-Nielsen, V.L. Kuchaev, J.H.B. Hansen, A.G. Zyskin, E.N. Shapatina, Journal of Molecular Catalysis A Chemical 315 (2010) 155–162.
[45] T. Chen, W. Wang, H. Miao, T. Li, C. Xu, Journal of Power Sources 196 (2011) 2461–2468.
[46] B. Novosel, M. Marinek, J. Maek, Journal of Fuel Cell Science and Technology 9 (2012).
[47] J.R. Rostrup-Nielsen, J. Sehested, Advances in Catalysis 47 (2002) 65–139.
[48] M. Andersson, F. Abild-Pederson, I. Remediakis, T. Bligaard, G. Jones, J. Engbæk, O. Lytken, S. Horch, J. Nielson, J. Sehested, J. Rostrup-Nielson, J. Nørskov, I. Chorkendorff, Journal of Catalysis 255 (2008) 6–19.
[49] J. Kuhn, O. Kesler, Relationships between Operating Conditions, Carbon Deposition, and Performance in Solid Oxide Fuel Cells. Ph.D. thesis, University of Toronto, 5 Kings College Rd, Toronto, ON, Canada, 2013.